

# Performance Enhancement of 157 nm Newtonian Catadioptric Objectives

James Webb, Timothy Rich, Anthony Phillips and Jim Cornell  
Corning Tropol Corporation, 60 O'Connor Rd, Fairport, NY 14450, 585-377-3200 (USA)

## ABSTRACT

Newtonian design forms have been developed to explore higher numerical aperture imaging systems at a wavelength of 157 nm with elements made of CaF<sub>2</sub> crystal. First-generation systems working at 0.60 NA are currently printing features smaller than 130 nm for resist-process-development. Second-generation design forms, working with variable numerical apertures above 0.75 NA, will push feature sizes significantly below 100 nm. Several aspects of second-generation designs have been improved to accommodate the need for characterizing and enhancing imaging performance. Closed-loop methods of optimization to reduce aberrations have been developed to characterize and control the effects of crystal-related birefringence on imagery. In addition these systems are learning vehicles to enhance knowledge of aberration-image performance dependence at high numerical apertures.

**Keywords:** microlithographic objective, CaF<sub>2</sub>, intrinsic birefringence, in situ compensation, 157nm, 193nm, catadioptric, Newtonian, aberration correction

## 1. INTRODUCTION

First-generation Newtonian 157 nm optical systems were built without the benefit of actinic wavelength interferometry or other methods for characterizing imaging performance at the wavelength of use. It was widely believed that single crystal CaF<sub>2</sub> material was isotropic and that off-wavelength (248 nm) optimization of the optical system using null testing techniques, similar to those developed for 193 nm systems, would suffice for producing systems at 157 nm.<sup>1, 2, 3</sup>

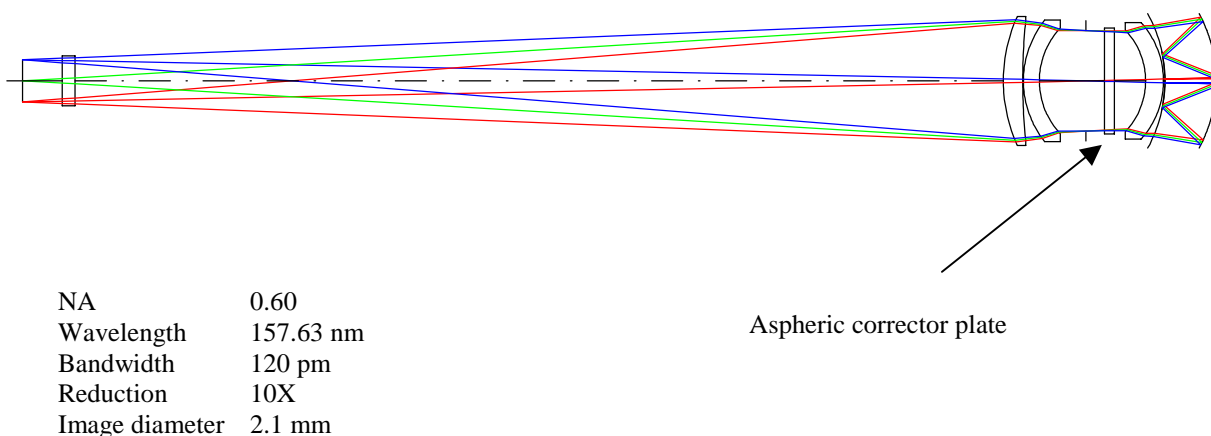


Figure 1. Small field Newtonian objective

Using off-wavelength testing techniques, system wavefronts are interferometrically measured at 248 nm through null components, which correct spherochromatic aberration. The optimization method makes iterative corrections to the wavefront by modifying the surface of an aspheric plate, as shown in figure 1. After several iterations,

the information obtained from the wavefront is used in conjunction with modeling software to predict the performance at 157 nm. Systems have been built in this way with 5 nm rms of measured wavefront error (less than 0.03 waves rms at 157 nm). The measurements in Figure 2 illustrate the system wavefront after each iteration of the optimization process.

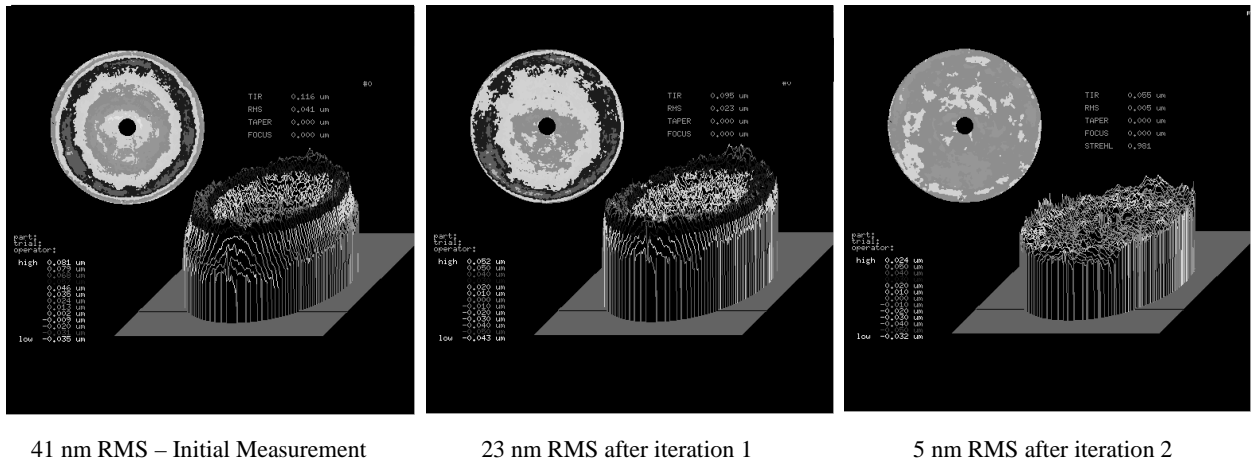


Figure 2. Closed loop wavefront optimization at 248 nm using null

Methods of analyzing aberration content of images in resist have been developed using lines of varying feature sizes and using phase rings<sup>4, 5</sup>. Line-width fidelity, limiting resolution and useable depth of focus for different types of features are obtained over the imaging field in resist. The dimensions are measured with the SEM. Methods have been developed to characterize the system imaging in terms of residual aberrations identified from information contained within these microscope images. Symmetric, 1- $\theta$ , 2- $\theta$ , 3- $\theta$  and field-dependent aberrations can be described using Zernike polynomials. These aberration measurements are used as input to modeling software<sup>6</sup> that predicts their effect on imagery. Residual aberrations that can compensate for the effects on imagery are computed and performance improvements determined.

Newtonian objectives are installed into step and repeat cameras and used for 157 nm photo resist process development. Figure 3 shows resist images from a mask with equal lines and spaces.

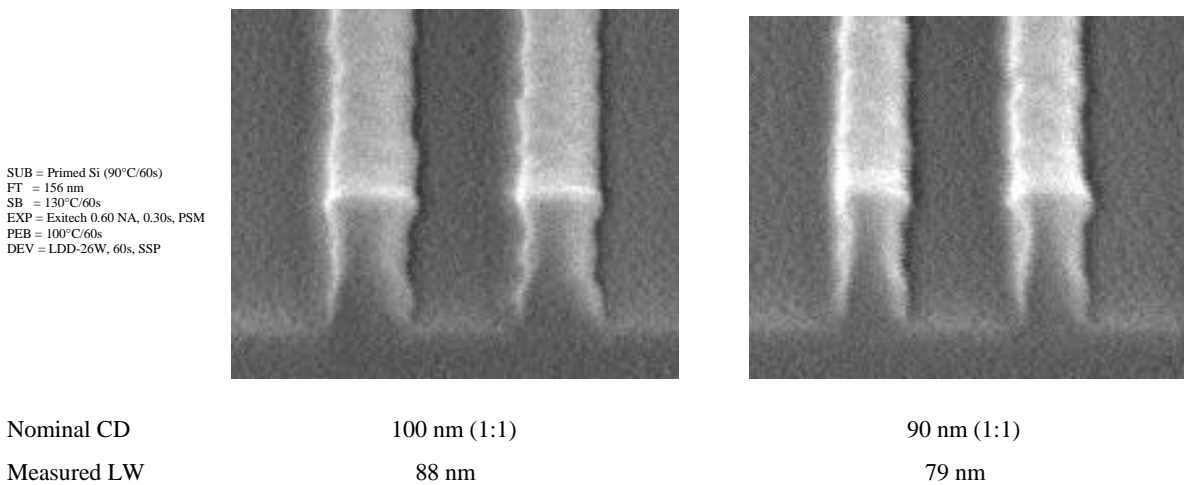


Figure 3. SEM images in resist courtesy of C. Bai of Shipley and J. Meute of International SEMATECH

## 2. INTRINSIC BIREFRINGENCE

Early attempts to measure wavefront errors using 157 nm interferometry on first-generation 0.60 NA systems gave indications of crystal-related birefringence effects. Birefringence creates in a lens, polarization-dependent phase errors and contrast problems when a lens is wavefront tested in a double pass configuration as shown in Figure 4. Complete loss of contrast can occur with a half wave of phase retardation. A crystal-orientation-dependent birefringence with less than half wave phase delay is observed.

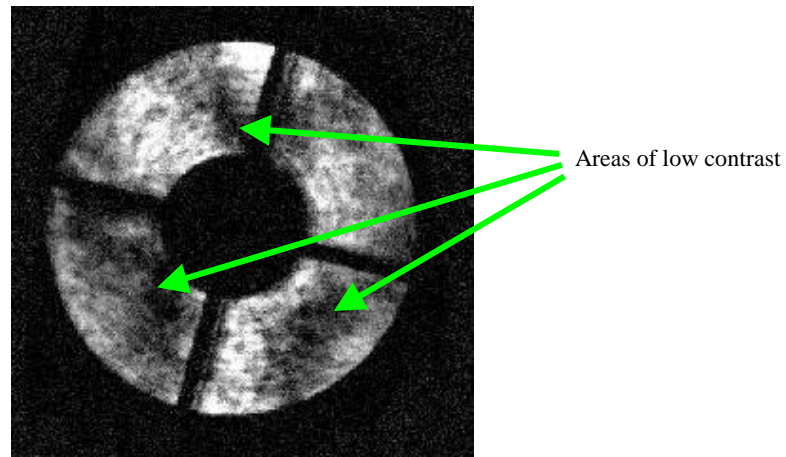


Figure 4. Interferometer fringe modulation plot through a 0.60 NA system viewed using a Schwarzschild feed objective

It is now known that calcium fluoride is not isotropic at 157 nm. There is intrinsic birefringence in the material that depends on crystal orientation as described in figure 5. This intrinsic birefringence was first quantified by researchers at NIST<sup>7</sup> as having a maximum value for light traveling in the [110] direction in the crystal, at an angle of 35.26° away from the [111] crystal axis.

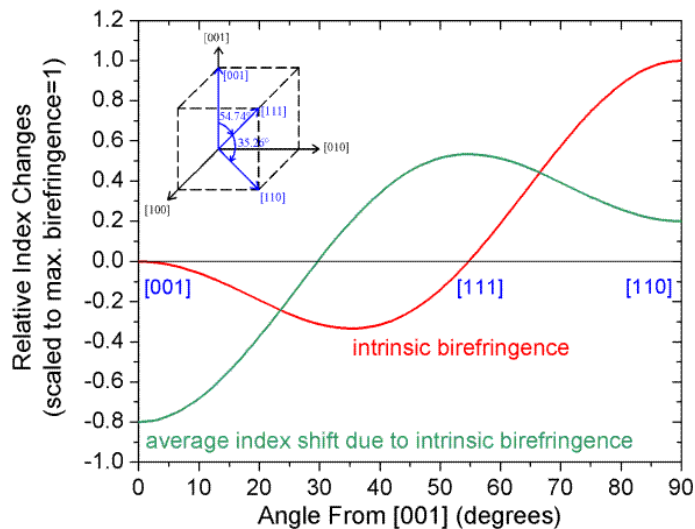


Figure 5. Intrinsic birefringence in calcium fluoride as a function of the direction of light propagation  
 Courtesy of John Burnett, Zachary Levine, and Eric Shirley, Plasma Radiation Group, NIST

There are eight {111}-crystal planes that describe an octahedron shape in CaF<sub>2</sub>, as shown in figure 6. The material used in our Newtonian objectives has the optical axis perpendicular to one of the (111) crystal orientation planes. The effect of the intrinsic birefringence on imagery varies as a function of the angle of light propagating through the material. In this orientation, symmetric and 3-θ polarization-dependent phase errors occur. Rays propagating through the crystal at angles greater than 35.36° from the optical axis and away from the <110> directions experience diminishing effects of birefringence. As ray angles increase to 54.74°, the effect of intrinsic birefringence vanishes in three locations oriented 60° apart and located half way between the <110> directions as shown in Figure 7.

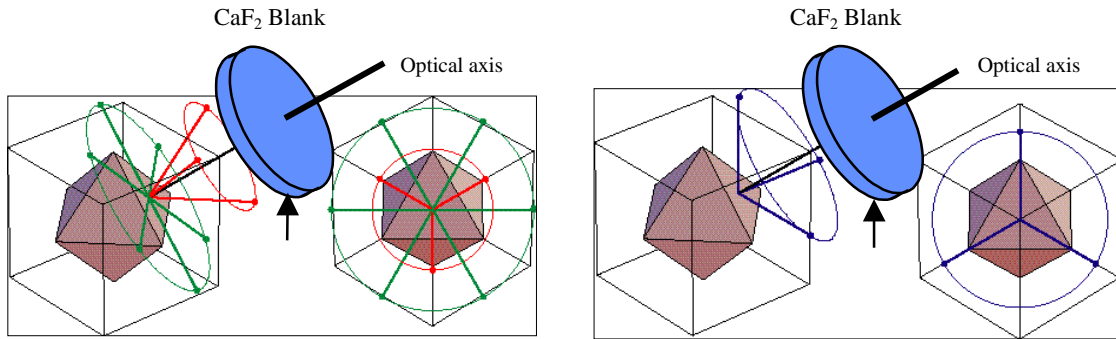
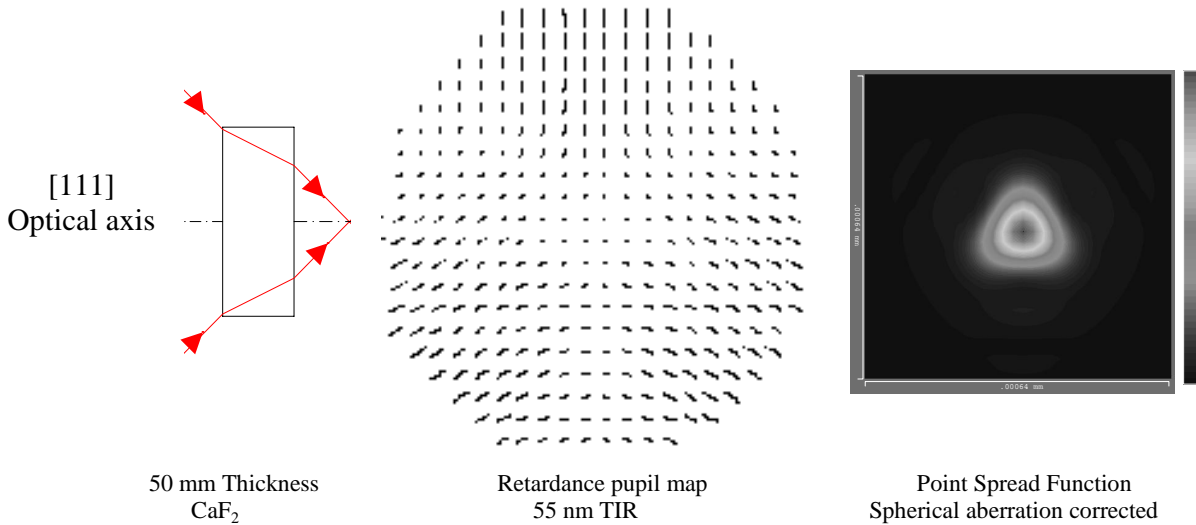


Figure 6. Optical axis, {111} planes and <110> directions      Figure 7. Optical axis, {111} planes and <100> directions

Angles beyond 40° are not normally possible for an all-refractive system imaging in nitrogen. There are special cases where reflection angles internal to the glass can be even greater than 54.74°. A special case is used in our Newtonian design.

Figure 8A shows a cone of light passing through a CaF<sub>2</sub> plate at an angle of 33° and forming an image at 0.85 numerical aperture. In Figure 8B each point in the pupil represents a different ray angle propagating through the crystal. The line in this retardance pupil map help to visualize the change in phase relationship within the lens pupil. The direction of each line indicates the orientation of the fast (lower index) axis and the length of the lines is a measure of the phase retardance.



50 mm Thickness  
CaF<sub>2</sub>

Retardance pupil map  
55 nm TIR

Point Spread Function  
Spherical aberration corrected

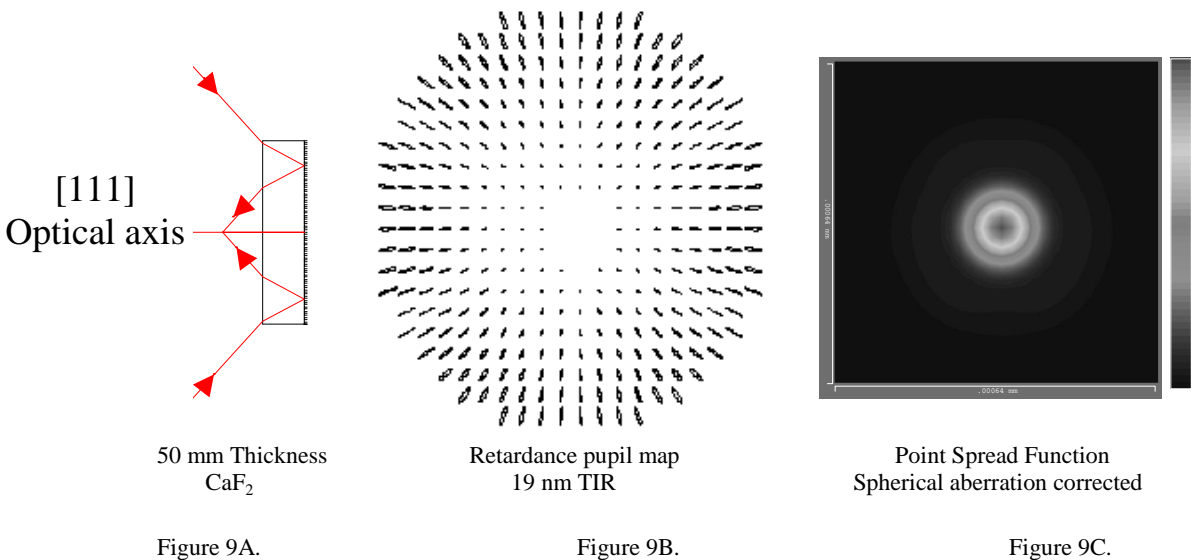
Figure 8A.

Figure 8B.

Figure 8C.

Figure 8C shows the effect that the intrinsic birefringence has on the image point spread function. In this example, the cone of light passing through a 50-mm-thick plate has been corrected for spherical aberration. The maximum phase retardance is 55 nm TIR (Total Indicated Retardance). This clearly shows both the substantial effect that the intrinsic birefringence has on imaging and the strong directional dependence it has to crystal orientation.

In Figure 9A, the light travels at the same cone angle and numerical aperture through a 25-mm-thick plate and is reflected at the second surface back through the material at opposite angles. The total glass path is the same in this case as in Figure 8A, but the effect on the phase and image point spread function is significantly different. Each pass through the material shows the 3- $\theta$  polarization-dependent phase errors seen above, but because the two angles through the plate are of equal and opposite sign, the asymmetries in the retardance are cancelled and only a symmetric birefringence remains. Figure 9B exhibits only 19 nm of radial birefringence, and Figure 9C shows the resulting radially symmetric image point spread function. This canceling property of the 3- $\theta$  birefringence in this example is beneficial to these Newtonian form lenses as described in greater detail later.



### 3. 0.85 NA 15X OBJECTIVE AT 157 NM

A second-generation optical design form as shown in Figure 10 has been developed to push 157 nm lithography below 100 nm. This design has many advanced features that provide the user with adjustment capability to control or improve pupil- and field-dependent aberrations.

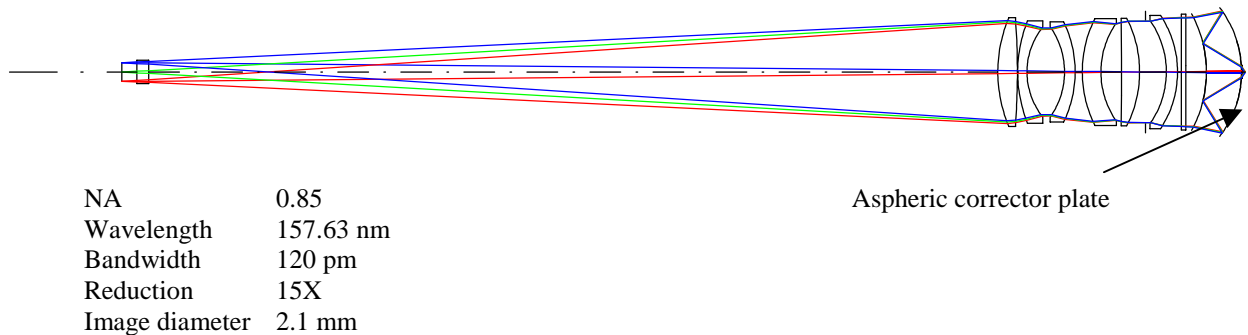


Figure 10. High NA Newtonian objective

157 nm interferometer wavefront testing capability was not available for the first 0.85 NA systems produced. With only qualitative knowledge that intrinsic birefringence can affect imaging performance and without design methods in place to quantify or modify their effect, the objective is designed with in situ adjustment capabilities. Figure 11 identifies the component locations for adjustments of field curvature, spherical aberration, and asymmetric, 1- $\theta$ , 2- $\theta$ , 3- $\theta$  wavefront modifications. These capabilities allow for improving performance based on in situ measurements of aberrations, or provide the ability to modify the aberration content of the system in a predictable fashion.

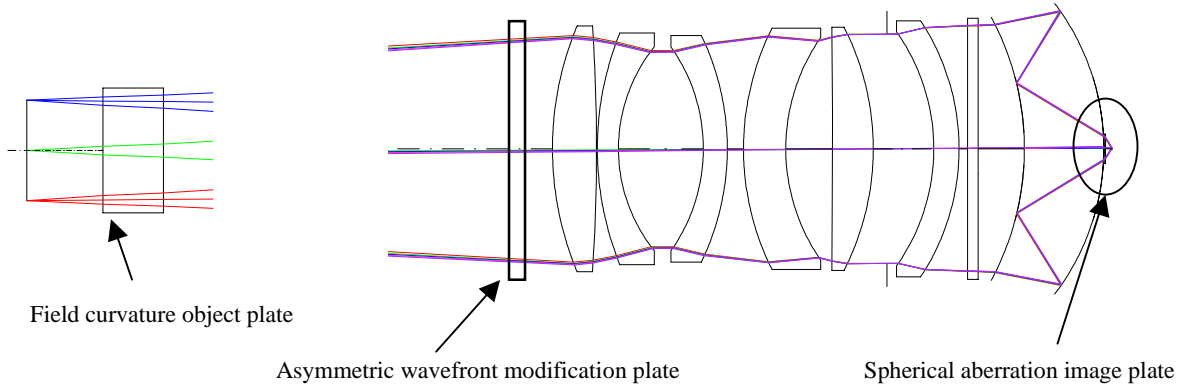
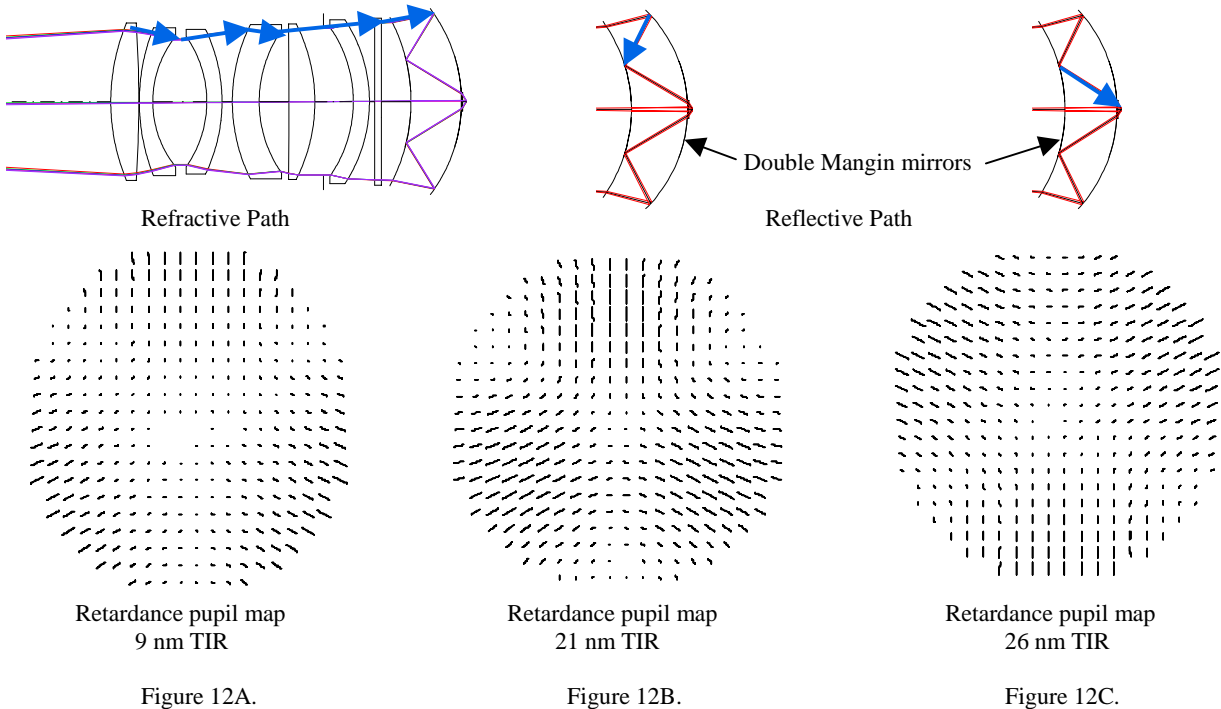


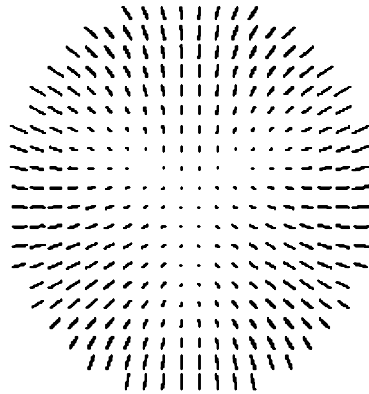
Figure 11. Field replaceable correction components

The 0.85 NA system consists of an optical path through the refractive group as shown in Figure 12A and two reflective passes within the Mangin mirror, as shown in figure 12B and 12C. The optical axis is normal to a [111] crystal plane for all the components, as is shown in figure 6



The refractive group of elements has an axial glass path of 52 mm with marginal ray angles less than 15°, and rays traversing this group do not accumulate significant amounts phase retardance from the intrinsic birefringence. In the worst case, even if each of the elements were clocked in orientation to maximize the phase retardance, the total

accumulated birefringence would be only 9 nm TIR. The first reflection internal to the Mangin mirror has a marginal ray angle within the crystal of  $58^\circ$ . The cone passing through the Mangin mirror accumulates the effects from all three-crystal directions. Zero birefringence for both [111] and [001] directions and 21 nm TIR of phase retardance in the [110] direction effects can be seen in figure 12B. The last pass through the Mangin crystal is the longest single glass path length for a marginal ray and accumulates 26 nm of phase retardance with a maximum marginal ray angle of  $32^\circ$  as shown in Figure 12C. The two reflected angles internal to the Mangin mirror are in opposite directions; therefore the accumulated  $3-\theta$  asymmetric portion of the intrinsic birefringence is significantly reduced. The total sum of the accumulated phase retardance from intrinsic birefringence for the entire lens system is 24 nm TIR, as shown in figure 13A.



Retardance pupil map  
24 nm TIR

Figure 13A.

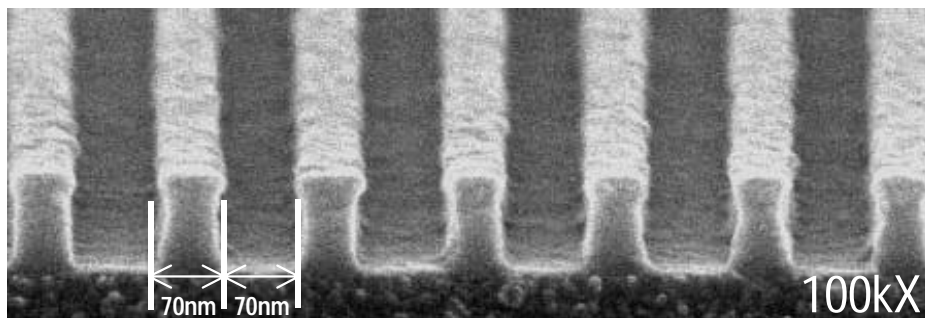


Point Spread Function  
Design aberrations included

Figure 13B.

The phase retardance degrades the performance of the aerial image. Another factor that degrades the performance at 157 nm is related to the off-wavelength optimization at 244 nm. There is an average index variation due to intrinsic birefringence that leaves a  $3-\theta$  asymmetric error in the wavefront at 157 nm. The combination of these effects reduces the peak contrast performance when compared to the performance without including intrinsic birefringence effects. The ratio of the peak contrast values provides a normalized contrast value of 91%. The point-spread function is shown in Figure 13B.

SEM performance data of the first 0.85 NA 157 nm system build is provided in Figure 14. The system was optimized using 244 nm null-correction interferometry. Equal lines and spaces with 70 nm resolution were easily achieved.



Nominal CD 70 nm (1:1) binary mask 0.7 sigma

Figure 14. SEM resist images of equal lines and spaces using a binary mask  
Courtesy of T. Itani of SELETE and M. Gower of Exitech

#### 4. METHODS OF COMPENSATION

It is possible to improve the performance of the system when wavefront measurements at 157 nm can be obtained. Figure 15 shows the uncompensated wavefront error due to the average index error caused by intrinsic birefringence. Compensation can be achieved by correcting the effects during the closed loop wavefront optimization at 157 nm using the internal asphere compensation plate. The plate can be modified to include the spherical and 3- $\theta$  asymmetric corrections necessary to reduce the wavefront errors.

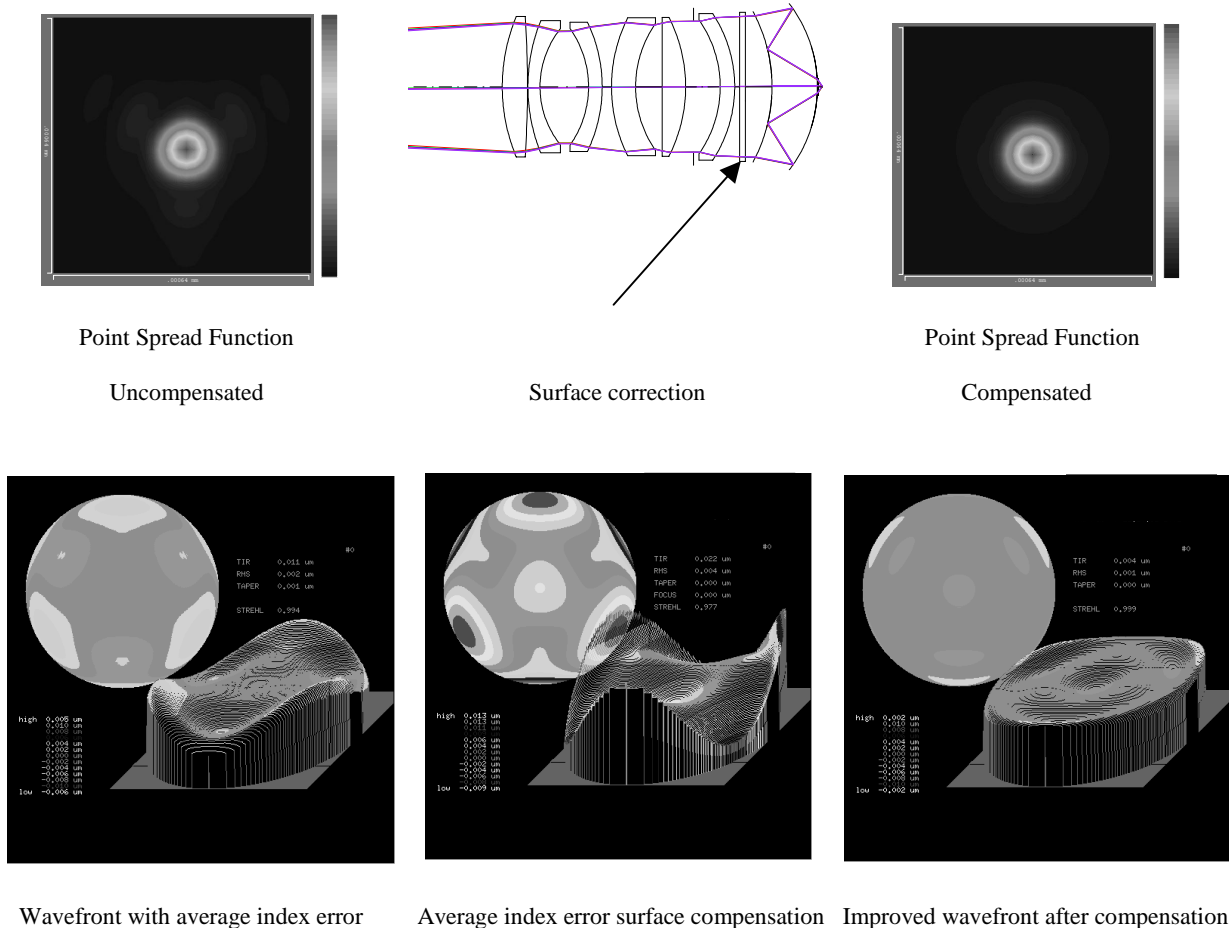
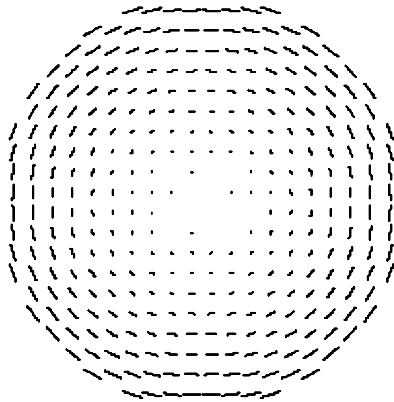


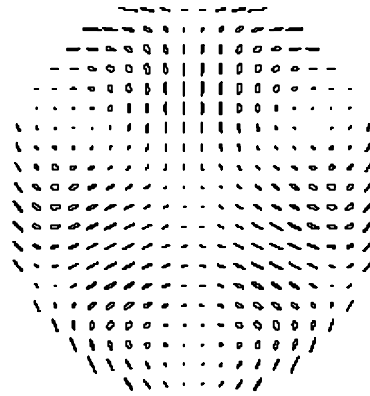
Figure 15. Average index wavefront correction

Reducing the phase retardance effects from intrinsic birefringence can make further improvements to the system performance. Modeling indicates that it is possible to introduce a phase compensation plate into the assembly similar to the wavefront modification plate described in Figure 11. A compensation plate with a radial phase retardance that is opposite in sign to that caused by the intrinsic birefringence can be inserted into the assembly. Figure 16A is an example of 20 nm radial phase retardance. When it is introduced into the assembly as a compensator the intrinsic birefringence effect can be reduced substantially. Figure 16B is the higher order residual birefringence that remains. The maximum phase retardance error after compensation is only 7 nm. The higher order residual is caused because the two passes within the Mangin mirror are at differing angles. The three areas within the pupil where the phase delays are reduced to zero are visualized by small dots in the retardance pupil map; correspond to the rays that pass through the [001] minimum intrinsic birefringence direction.



Retardance pupil map  
20 nm TIR

Figure 16A.



Retardance pupil map  
7 nm TIR

Figure 16B.

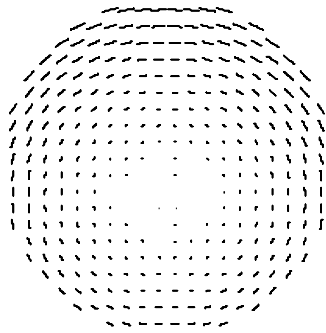
The normalized contrast improves to 98.1% of the original performance, as shown in figure 17, by reducing the average index wavefront error and by reducing the phase retardance that are caused by the intrinsic birefringence.



Point Spread Function  
Average index wavefront and Phase retardance aberrations reduced

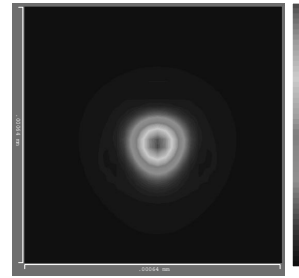
Figure 17.

There may be other crystal-orientation-related factors that can influence imaging performance. Correction of phase-delay errors in the assembly may not be limited to the intrinsic birefringence errors calculated when the optical axis of the elements coincides with the crystal axis. For example, blank fabrication and component processing may lead to a small crystal axis tilt relative to the optical axis. This will lead to a  $1-\theta$  asymmetric error in the phase delay.



Retardance pupil map  
20 nm TIR

Figure 18A.



Point Spread Function  
Asymmetric phase retardance

Figure 18B.

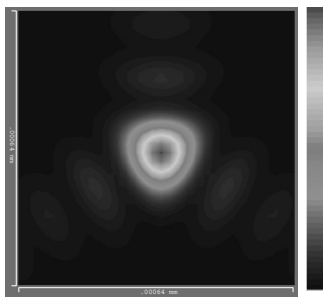
Figure 18A is an example of a type of asymmetric phase delay error that can be created from a crystal axis tilt. The asymmetric effect on the aerial image is shown in figure 18B. An asymmetric compensating plate can be used to reduce this phase delay error. Other low order types of phase compensation are possible.

## 5. MEASUREMENT TECHNIQUES

Unpolarized and multiple orientations of linearly polarized measurements of the wavefront using 157 nm interferometry are used to determine the type of compensation necessary in the optical assembly. Examination of the x and y Zernike components of the aberrations in the measured wavefronts provide the information necessary to determine the amount of surface and phase delay compensation on a correction plate that will best improve performance.

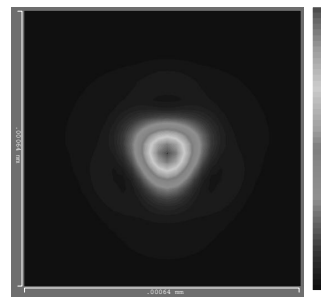
Figure 19A and 19B are examples of aerial images that have a similar image shape distortion. The point-spread function in figure 19A was created by introducing a 3- $\theta$  asymmetric surface error to a modification plate. A similar point spread function in figure 19B was created using a 3- $\theta$  asymmetric phase delay on a modification plate. Examination of Zernike polynomial fits to the wavefront using both an x and y oriented polarization analyzer are listed in tables 1A and 1B.

A surface correction can be used to improve the wavefront when the average of x and y Zernike coefficients is of a substantial value and the difference in x and y Zernike coefficients is near zero. Improvement can occur if both the x and y polarization Zernike values are reduced.



Point Spread Function  
3- $\theta$  Zernike surface error

Figure 19A.



Point Spread Function  
3- $\theta$  Phase retardance error

Figure 19B.

In contrast, a phase delay correction can be used to improve the wavefront when the difference of x and y Zernike coefficients is of substantial value and the average of the x and y Zernike coefficients is near zero. Again improvement can occur if both the x and y polarization Zernike values are reduced.

### Zernike Polynomials

	POL_X	POL_Y	AVG_X_Y	DIFF_X_Y
1	0.0000	0.0000	0.0000	0.0000
2	0.0000	0.0000	0.0000	0.0000
3	0.0000	0.0000	0.0000	0.0000
4	-0.0379	-0.0376	-0.0377	0.0003
5	-0.0022	0.0022	0.0000	-0.0044
6	0.0000	0.0000	0.0000	0.0000
7	0.0000	0.0000	0.0000	0.0000
8	-0.0001	0.0000	-0.0001	-0.0001
9	-0.0012	-0.0010	-0.0011	-0.0002
10	0.0000	0.0000	0.0000	0.0000
11	0.3091	0.3090	0.3090	0.0001

Table 1A.

### Zernike Polynomials

	POL_X	POL_Y	AVG_X_Y	DIFF_X_Y
1	0.1440	0.1536	0.1488	-0.0096
2	0.0000	0.0000	0.0000	0.0000
3	-0.1258	0.1236	-0.0011	-0.2494
4	-0.0777	-0.0652	-0.0714	-0.0125
5	-0.0669	0.0673	0.0002	-0.1342
6	0.0000	0.0000	0.0000	0.0000
7	0.0000	0.0000	0.0000	0.0000
8	0.0107	-0.0116	-0.0004	0.0223
9	0.0032	0.0051	0.0042	-0.0019
10	0.0000	0.0000	0.0000	0.0000
11	-0.0019	0.0338	0.0160	-0.0357

Table 1B.

When both the average of the x and y polarization Zernike values and the difference of the x and y polarization Zernike values are large, then correction using both methods of compensation is required.

## 6. CONCLUSIONS

Several systems have been built and tested with off-wavelength 248 and 244 nm interferometry that did not identify or compensate for the effects of intrinsic birefringence. Resist images from these systems demonstrate performance that is beneficial for resist development and exceeds the resolution specification.

Second generation Newtonian objectives have been developed which incorporate methods of adjustment and compensation for intrinsic birefringence effects. These objectives have advanced capabilities to study aberration effects on imagery. Effects of intrinsic birefringence in the optical materials have been quantitatively modeled. These models show that improvement in performance is possible with compensators for wavefront and birefringence aberrations.

## ACKNOWLEDGEMENTS

The authors would like to thank David Aronstein, John Bruning, Lisa Rich and Horst Schreiber for their help in completing this manuscript.

## REFERENCES

1. Patent No. 5,650,877 Imaging System for Ultraviolet Lithography.
2. J.E. Webb, et al., "Optical Design Forms for DUV&VUV Microlithographic Processes", SPIE Vol. 4346\_55, Optical Microlithography, pp 566-567, 2001.
3. S. Mack, et al., "Error separation technique for microlithographic lens testing with null configurations", SPIE Vol. 4346\_139, Optical Microlithography, pp1328-1339, 2001.
4. C. M. Garza, et al., "Ring test aberration determination & devise lithography correlation", SPIE Vol. 4346\_5, Optical Microlithography, pp 36-43, 2001.
5. J. P. Kirk, et al., "Aberration measurement using in situ two beam interferometry", SPIE Vol. 4346\_2, Optical Microlithography, pp 8-14, 2001.
6. Intrinsic birefringence and imaging simulations were carried out using Optical Research Associates, CodeV version 9.02β.
7. J. Burnett, et al., "Intrinsic Birefringence in 157 nm Materials", SEMATECH Calcium Fluoride Birefringence Workshop, 18 July 2001, San Francisco, CA.